Measurement of the Astronomical Unit

Umran Haji
*University of California, Berkeley, Department of Astronomy**

We estimate the astronomical unit by measuring the rotation period, angular size, and rotation speed of the sun. We measure the rotation period by tracking sunspots in a video from the Solar and Heliospheric Observatory (SOHO) spacecraft, finding a period of 22.82 ± 0.22 days. The angular size and rotation speed are found from optical spectra of the sun taken on November 7, 2018 and ephemeris data from JPL Horizons; by fitting an Eddington limb-darkening profile to flux data, we find the duration of the line of sight's transit of the solar disk, and use the known declination of the sun to find an angular size of 0.420 ± 0.006 degrees. Finally, from Doppler shift measurements and solar ephemerides, we find a rotation speed of 1.95 ± 0.01 km/s. We calculate an AU value of $1.69 \pm 0.03 \times 10^8$ km.

I. INTRODUCTION

The Earth-Sun distance D can be easily calculated if one only knows the angle θ subtended by the sun and its physical size, using the relation $\theta = 2R_\odot/D$. We set out to do exactly this. Under the approximation that the sun rotates as a rigid body, the radius $R_\odot$ can be related, by $v = 2\pi R_\odot/P$, to the rotation period P and speed v, both of which can be measured.

The sun's period P can be measured by tracking sunspots across the solar disk, measuring the time it takes for them to traverse a given angular distance, and extrapolating to the full period. Meanwhile, to determine θ and v, we take observations of the sun by fixing a telescope to point at the sun's declination and just "ahead" of the sun in right ascension, allowing the sun's diameter to pass through the line of sight. The sun's angular size is found from the ratio of the transit duration to the length of the solar day. Finally, we use spectra from the transit to find the radial velocity along the line of sight as a function of time and thereby find the rotation speed. Combining all of our observed quantities yields an estimate for the AU.

II. SOLAR ROTATION PERIOD

The first step in our analysis is to determine the rotation period of the sun by tracking sunspots in a video of the sun by the SOHO spacecraft.

There is a paucity of equatorial sunspots that survive for an entire trek across the solar disk; some disappear during the transit while others appear in the middle of it. Thus, to collect more data points at the cost of larger uncertainty on each data point, we track equatorial sunspots for approximately one quarter of a period. i.e., we track sunspots as they pass either from the eastern (left) edge of the solar disk to the center, or from the center to the western (right) edge.

To accurately measure the period, we must account for the motion of SOHO with the sun. The scenario is diagrammed in Figure 1. Suppose the spacecraft starts at position A and observes a sunspot at point P_1 at the apparent center of the solar disk. The sun rotates counterclockwise, and thus so does the line from the sun to SOHO, which is located at the L_1 Lagrange point. If the spacecraft were not moving with respect to the sun, one could determine the length of time it takes the sunspot to make a quarter of a rotation by simply waiting until the sunspot moves from P_1 to P_3. That is to say, the sunspot will disappear over the edge of the solar disk when it reaches P_3.

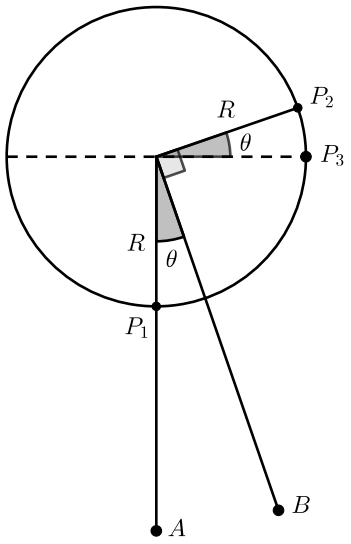

FIG. 1. The geometry of how the SOHO spacecraft has moved with respect to the sun during an observation. The sun rotates counterclockwise. A and B represent two different positions of the spacecraft. We seek to measure the time it takes a sunspot to move from P_1 to P_3. In reality, by the time the sunspot disappears from view, it is at P_2.

However, in reality, the spacecraft is "moving" with the sun, and hence the point at which the sunspot disappears from the spacecraft's view occurs *not* at P_3, but instead at some point P_2 "ahead" of P_3. Thus the time measured between the moment when a sunspot appears at the center of the disk and the moment when it disappears over the edge is *greater than* one quarter of a

* uhaji@berkeley.edu

period.

We correct for this as follows: Let D_{13} be the arc length from point P_1 to P_3 and D_{12} be the arc length from P_1 to P_2. By the time the sunspot has disappeared over the edge, SOHO has moved by an angle θ. Observe that

$$D_{12} = R\left(\theta + \frac{\pi}{2}\right)$$
$$D_{13} = R\frac{\pi}{2}$$

and hence

$$\frac{D_{12}}{D_{13}} = \frac{\theta + \pi/2}{\pi/2} \tag{1}$$

Since the sun is assumed to be rotating at a constant speed for a given latitude, the ratio in (1) is the factor by which the elapsed time between P_1 and P_2 is greater than one quarter of a period. That is to say, letting Δt be the time elapsed between P_1 and P_2 and letting P be the period,

$$\Delta t = \left(\frac{\theta + \pi/2}{\pi/2}\right)\frac{P}{4} \tag{2}$$

Now, since the spacecraft is located at L_1, its orbital period is the same as Earth's, and hence the angle θ can be related to the fractional distance it has traveled in its orbit during the time Δt, i.e.

$$\theta = 2\pi\,\frac{\Delta t}{365} \tag{3}$$

where Δt is in days.

Combining (2) and (3), we obtain an extrapolated value of P given an observed Δt:

$$P(\Delta t) = 4\,\Delta t\left(\frac{\pi/2}{2\pi\,\dfrac{\Delta t}{365} + \pi/2}\right) \tag{4}$$

The math is identical when the sunspot starts at the edge and moves to the center.

We observed eight sunspots as they traversed an apparent quarter of the sun, calculated the time Δt that each one took, and used equation (4) to extrapolate a period. To obtain uncertainties, for each sunspot, we advanced the video frame-by-frame and found two points in time such that we were all but certain that the sunspot was at the start of its quarter-circumference journey between those two points. Those two points were then used to define a 2σ region for the start time. We did the same for the end of each sunspot's journey.

As the measurement of the start time is independent of that of the end time, adding the uncertainties in quadrature and applying the propagation of error formula to equation (4) yields the error bars in Figure 2, wherein we show extrapolated periods for each sunspot.

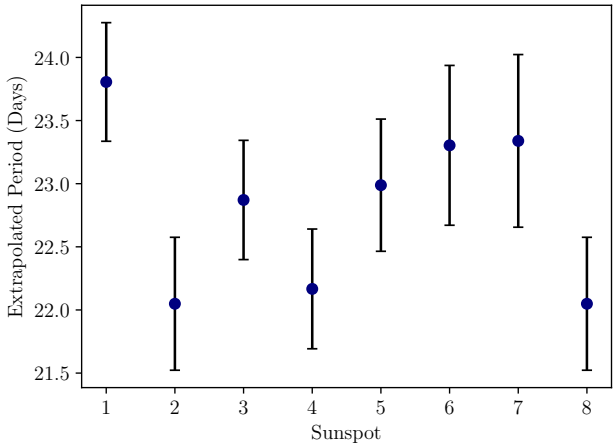

FIG. 2. Extrapolated solar equatorial periods, calculated from observing apparent quarter-periods of eight sunspots.

By averaging the extrapolated periods and using the standard deviation of the mean for independent observations, we find an equatorial period of 22.82 ± 0.22 days.

III. ANGULAR SIZE OF THE SUN

We took approximately 30 spectra of the sun by using a small optical telescope to project the image of the sun onto a plate, collecting the light via a fiber optic cable held in place in a hole in the plate and connected to a spectrograph in a dark room. We also took several exposures before and after the transit, as well as "dark" images and flat-field spectra of a halogen lamp to correct the solar spectra. In this section, we use the integrated flux data from our spectra to determine the duration of the transit of the sun's image across the "aperture" of the fiber optic cable, and from this determine the sun's angular size. First, we estimate the transit duration as a parameter in the limb-darkening profile of the solar disk.

Under the Eddington model for the solar atmosphere, we expect the observe brightness I to be given by

$$I = I_0\frac{2 + 3\cos\alpha}{5}$$

for some peak brightness I_0, where α is the angle between the line of sight and the vector normal to the solar surface. This can be rewritten in terms of time t as

$$I(t) = \frac{I_0}{5}\left(2 + 3\sqrt{1 - \left(\frac{t - t_0}{\Delta t}\right)^2}\right) \tag{5}$$

where Δt is the duration of the transit and t_0 is the point at which the center of the solar disk is in view.

Figure 3 shows the total brightness of each solar scan image as a function of time elapsed from an arbitrary

starting point a few images before the sun is in view. Before calculating the brightnesses, we dark-subtract each image and divide by a normalized average flat-field from the halogen lamp. We fit the model in equation (5) by least-squares, finding good agreement with the data.

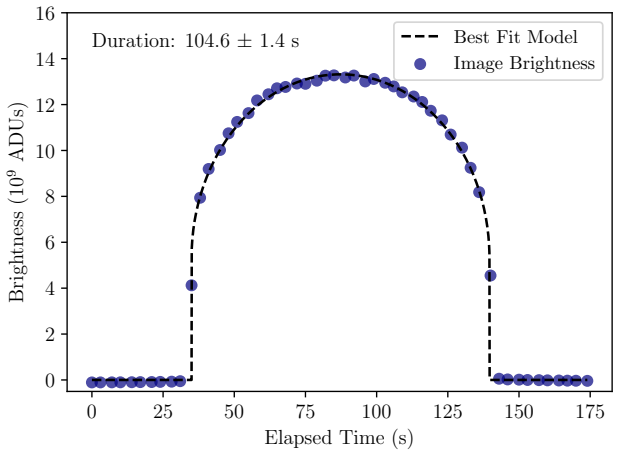

FIG. 3. Total brightness across the entire CCD as a function of elapsed time from an arbitrary starting point before the transit. The dashed line is the best-fitting Eddington model, from which we estimate the transit duration.

We find a transit duration of 104.6 ± 1.4 seconds. To deduce from this an angular diameter θ, we note that the angular speed of the sun across the sky is the "angular" circumference of the circle it traverses on the sky divided by the length of a solar day, i.e. 24 hours. Since the sun is at some nonzero declination δ, the circle it traverses has a circumference $2\pi\cos\delta$. Hence the angular speed of the sun is $2\pi\cos\delta/(24\text{ hours})$, and thus

$$\theta = \left(\frac{2\pi\cos\delta}{24\text{ hours}}\right)\Delta t \tag{6}$$

In our final calculation of the AU in section V, we substitute equation (6) for θ and thus do not need to calculate θ explicitly. However, we provide it here for completeness: At the time of our observation, $\delta = -16.4$ degrees according to the JPL Horizons system. Hence, we obtain

$$\begin{gathered}\theta = 0.420\text{ degrees} \\ \sigma_\theta = \sqrt{\left(\frac{2\pi\cos\delta}{24\text{ hours}}\right)^2\sigma^2_{\Delta t}} = .006\text{ degrees}\end{gathered} \tag{7}$$

IV. DETERMINATION OF THE SOLAR ROTATION SPEED

A. Processing of Spectra

Determining the rotation speed of the sun requires spectroscopic analysis. In this section, we discuss our preparation of the spectroscopic data.

The spectrograph disperses the collected light into several "orders" on the CCD, which must be turned into one-dimensional spectra in order to search for Doppler shifts. Figure 4 shows a spectrum taken from the center of the solar disk.

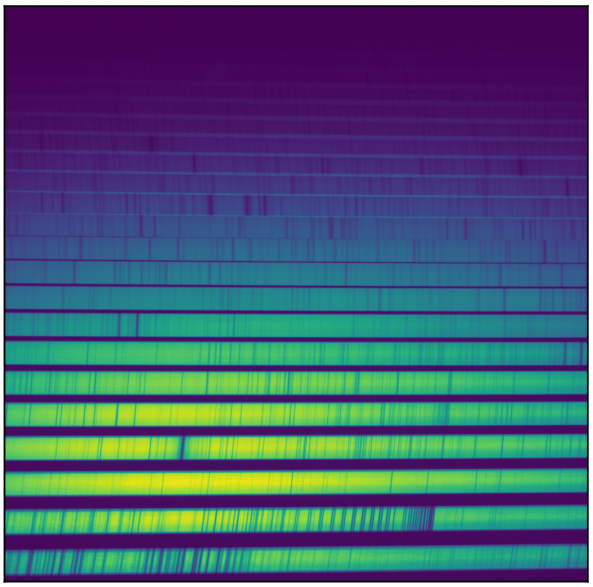

FIG. 4. The raw image of a solar spectrum. Note the shearing of the lines, an artifact of the optics. The fourth order from the bottom of the image is later used for wavelength calibration and Doppler shift detection.

1. *Correction of Shearing*

Due to the geometry of the optics, the spectrum is tilted in various ways on the CCD. In particular, many orders have a significant "shearing", which will compromise spectral resolution if one extracts a 1-D spectrum by simply summing each order over the vertical axis. To perform effective Doppler spectroscopy, maximum spectral resolution is desired.

To mitigate this problem, we apply linear shear transformations to several orders of the solar spectrum from Figure 4. Within each order, we determine an optimal correcting transformation by tuning the shear angle so as to maximize the depth of the deepest absorption line. This tends to increase the depths of other lines as well.

As it turns out, the actual deformation due to the optics is nonlinear, and the optimal shear angle for one line in an order is in general *not* the same as the optimal shear angle for other lines. Nevertheless, this first-order correction yields substantially improved spectral resolution for relatively little effort.

Figure 5 shows the effect of applying the transformation to one order of the solar spectrum (the fourth order from the bottom in Figure 4).

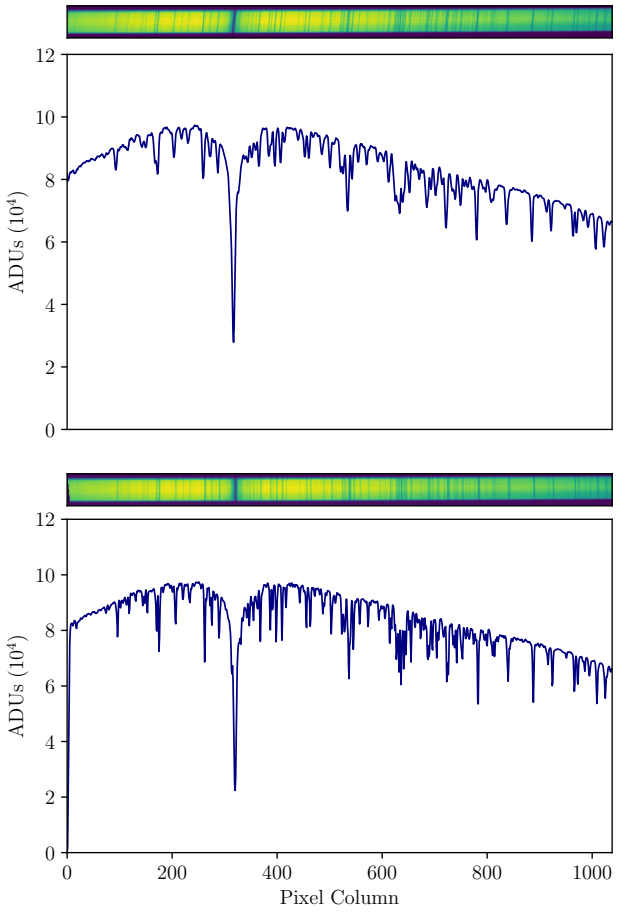

FIG. 5. We apply shear transformations to the 2D spectrograph images to improve absorption line sharpness and thus spectral resolution. The top plot shows a "raw" image of one order and its one-dimensional "collapsed" spectrum. The bottom plot shows the same order with the correction applied. Edge effects are removed before undertaking further analysis.

The top plot shows the 2D image of the order, followed by the result of summing it over the vertical axis. The bottom plot shows the same order with the optimal transformation applied.

Since applying the shear above also shifts the entire spectrum to the left, it is important to apply the *same* transformation to every image in order to avoid introducing spurious "Doppler shifts". We therefore save the matrix associated with the optimal shift in the solar spectrum and use it as a "master" transformation, applying it to the same order from all other images in our data set.

2. *Wavelength Calibration*

We obtain a wavelength solution for one order of the spectrograph by using a 653-nm laser and emission lines from a neon lamp. The laser appears in the same order that is fourth from the bottom of Figure 4. Additionally, three neon lines appear therein. In Figure 6, we show the summed spectrum for this order in the laser image, overplotted with that of the neon image (the shear correction from section IV A 1 is applied before extracting the 1D spectra). The laser is used to identify the neon lines. Each line is marked with its known wavelength in nanometers from [1].

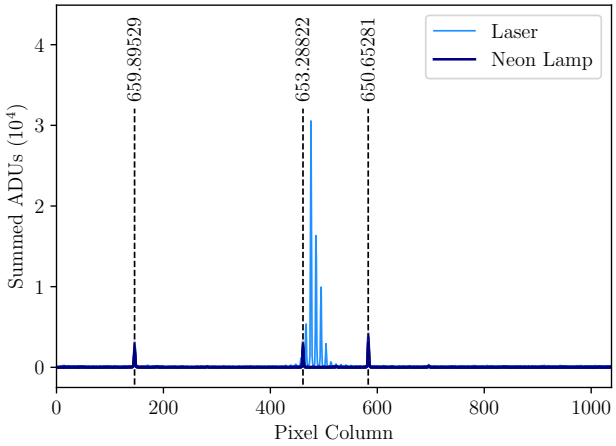

FIG. 6. Spectrum of 653-nm laser, overplotted with the same order from the spectrum of a neon lamp. The laser is used to identify three neon lines (labeled with wavelengths in nm) for wavelength calibration of the spectrograph.

We obtained 40 exposures of the neon lamp. To construct a wavelength solution and obtain uncertainties for it, we take advantage of the fact that we have 40 exposures at our disposal; Figure 7 is a zoomed-in version of Figure 6 showing the profile of one of the neon lines in each of the 40 different neon spectra. Calculating the centroid of this line in each of the 40 spectra yields Figure 8, an an empirical sampling distribution for this centroid. We determine the empirical sampling distribution of each of the three neon lines and then conduct a bootstrap procedure to construct a wavelength-vs-pixel polynomial fit; in each bootstrap trial, we draw one value, with replacement, at random from each of the three neon emission lines' empirical sampling distributions and fit a quadratic polynomial to the resulting three points. Performing several thousand trials yields a distrbution of possible wavelength solutions.

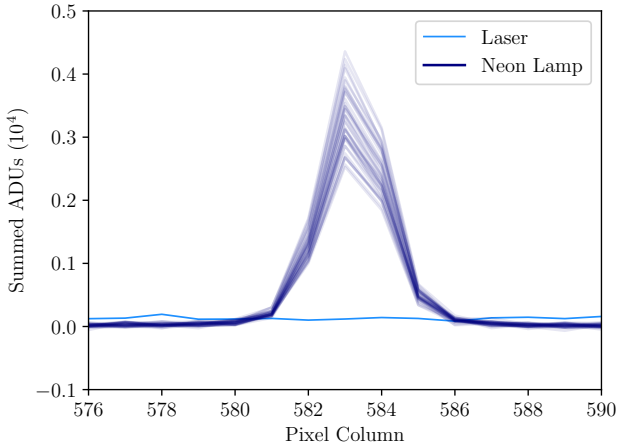

FIG. 7. A close-up of a neon line in Figure 5. Spectra of 40 exposures of the neon lamp are overplotted, showing the random uncertainty of the line profile.

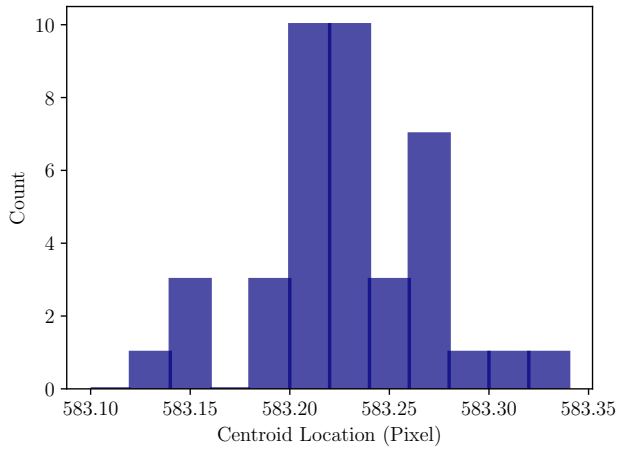

FIG. 8. The sampling distribution of the centroid of the neon line from Figure 7. The lines' centroids' sampling distributions are used as the basis for bootstrapping a wavelength calibration.

Our rationale for using a quadratic rather than a linear wavelength calibration is shown in Figure 9, in which we overplot the residuals from all of the bootstrap fits. Each cluster of points represents the sampling distribution of the centroid of one of the three neon lines. We see from the plot that each centroid's sampling distribution is very compact, i.e. each centroid's standard error is very small compared to the deviations from the fit. Hence, we conclude that the deviations are systematic rather than random errors, and thus it is not reasonable to model the wavelength solution as a straight line.

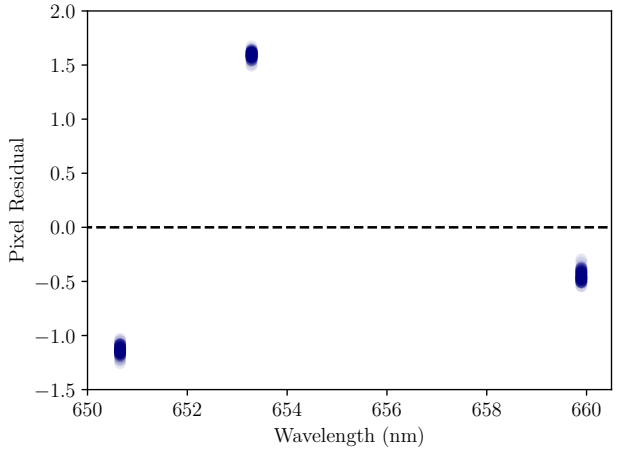

FIG. 9. Overplotted residuals from each bootstrapped first-order wavelength polynomial. The small spread in centroid position for each line compared to the magnitude of the residuals indicates that a linear fit deviates systematically from the neon emission lines. A quadratic fit is more appropriate.

Figure 10 shows the mean locations of the three centroids, overplotted with 100 of the bootstrap polynomial fits (which lie very close together and are hence indistinguishable in the plot).

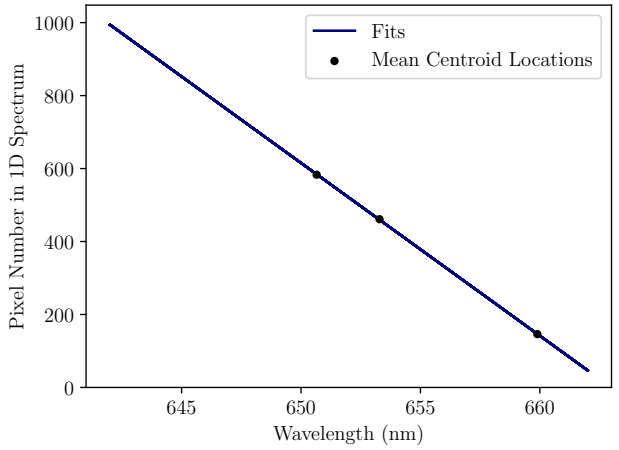

FIG. 10. 100 overplotted bootstrap wavelength polynomials.

B. Doppler Shift Detection

Upon obtaining spectra via the process described in section IV A, we use the method of cross-correlation to detect the Doppler shifts from the traversal of the sun's image across the line of sight. First we apply a square windowing function to each spectrum to neutralize edge effects when computing the cross-correlation function (CCF). An example is shown in Figure 11.

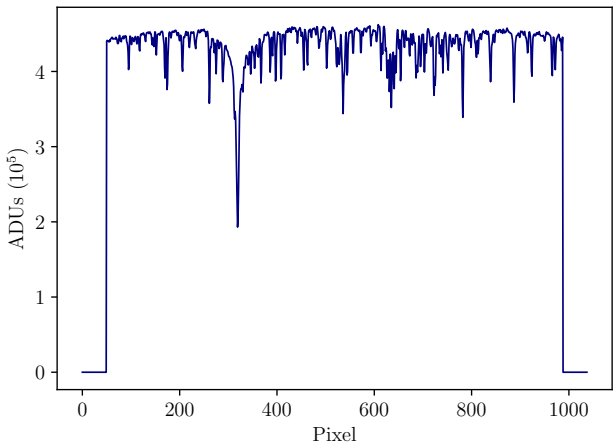

FIG. 11. A section of a 1D solar spectrum, with a square window applied to make the spectrum go to zero at the edges in preparation for cross-correlating.

A template is created by averaging all of the spectra taken of the solar disk, and the CCF of each solar spectrum with respect to that template is computed individually. The shifts caused by the sun's Doppler effect are much smaller than the width of a pixel, and hence we use an interpolation method to find the peak of each CCF. In each CCF, the three points around the maximum lag are fit by a parabola, and the analytically-determined vertex of the parabola is taken as the actual peak of the CCF. An example is shown in Figure 12.

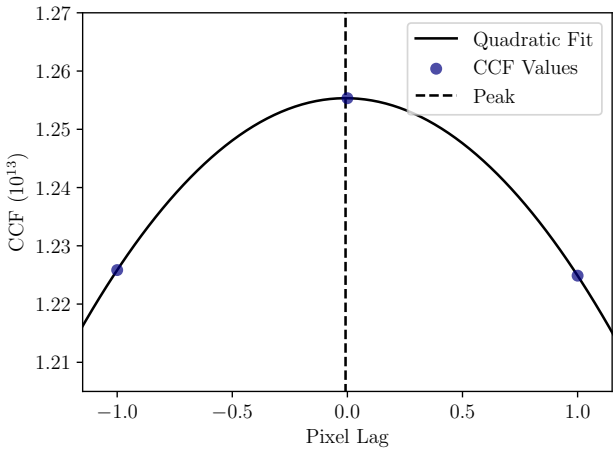

FIG. 12. Our method for determining the "true" sub-pixel shift of a solar spectrum. We fit a parabola to the three points around the peak of the CCF and solve for the vertex of the parabola, using this vertex, marked by the dashed line, as the shift.

Using this method to find the CCF peaks in all of our solar spectra yields the result in Figure 13.

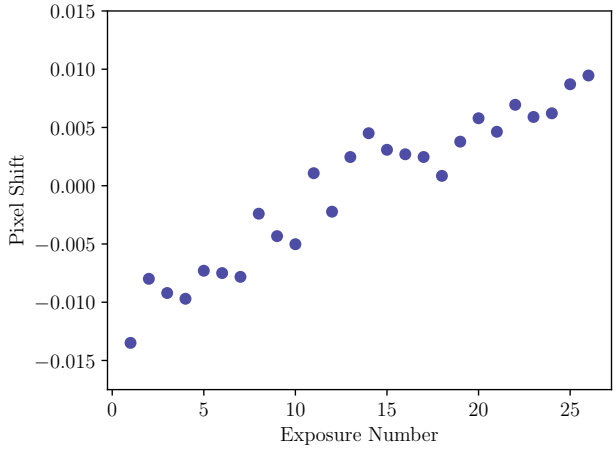

FIG. 13. The shifts of each solar spectrum relative to the average. Shifts are calculated using the method shown in Figure 12.

The next step is to convert the pixel shifts to wavelength shifts using our wavelength solution from section IV A 2. There is uncertainty in the wavelength shift caused not only by the fact that the wavelength solution is itself uncertain, but also by the fact that the wavelength solution is not linear with respect to the pixel numbers.

We investigated these sources of uncertainty and found that the variability associated with the conversion to wavelength space is extremely small in comparison to the variability originating from finding the peaks in the CCF; the scatter of the points about the trend in Figure 13 corresponds to a much larger uncertainty in Doppler shift than is accounted for by our propagated uncertainty from the conversion to wavelength space (these larger, empirical uncertainties are deferred to in section IV C where we estimate the sun's rotation speed). As a result, we simply used one of our wavelength polynomials to make the conversion of pixel shifts to values of $\Delta\lambda/\lambda_0$, estimating $\Delta\lambda$ using the average slope of the wavelength polynomial within the order and using the average wavelength value in the order as λ_0. Multiplying the results by the speed of light yields radial velocities for each exposure.

C. Rotation Speed Model-Fitting

The final step in determining the solar rotation speed is to fit our model, described in Appendix A, for the observed radial velocity as a function of position along the apparent equator, the sun's rotation speed, and the solar tilt relative to Earth, under the assumption of rigid-body rotation. Since the solar tilt is known from JPL data, and the positions along the equator of the points that were imaged in each exposure are known by comparing each file's timestamp to the start time of the transit, this amounts to fitting a one-parameter model to determine

the rotation speed v, which the rigid-body assumption allows us to identify with $2\pi R_\odot/P$.

Figure 14 shows the shifts plotted as apparent radial velocities, overplotted with the best-fitting model, which we fit by least-squares. Before fitting the model, we give each point an uncertainty of 0.25 km/s, estimated empirically based on the spread of the points about the trend. We find a rotation speed of 1.95 ± 0.01 km/s.

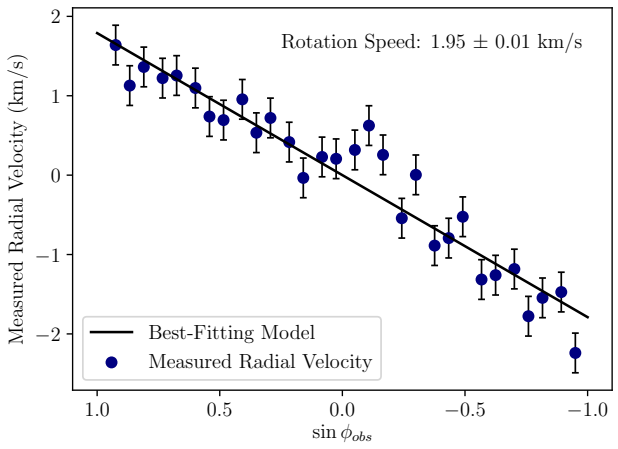

FIG. 14. Radial velocity as a function of $\sin\phi_{obs}$, where ϕ_{obs} is the "apparent" azimuthal angle of the point on the sun's surface that is being imaged; ϕ_{obs} lies in the apparent equatorial plane of the sun. See Appendix A for details. The horizontal axis is inverted so that time increases from left to right.

V. CALCULATION OF THE ASTRONOMICAL UNIT

We now combine our results to estimate the astronomical unit. From the JPL Horizons system, we find that the Earth was 0.99089 AU away from the sun at the time of our observation. Hence, by the small angle approximation $\tan\theta \approx \theta$, we relate this to the radius of the sun and its angular size by

$$\theta = \frac{2R_\odot}{0.99089 \text{ AU}}$$

$$\begin{aligned} 1 \text{ AU} &= \frac{1}{0.99089} \cdot \frac{2R_\odot}{\theta} \\ &= \frac{1}{0.99089} \cdot \frac{2(vP/2\pi)}{(2\pi\cos\delta/24 \text{ hours})\Delta t} \\ &= \frac{1}{0.99089} \cdot \frac{vP}{2\pi^2\cos\delta} \cdot \frac{24 \text{ hours}}{\Delta t} \end{aligned}$$

Consolidating all the unmeasured quantities yields

$$1 \text{ AU (km)} = 4604.66 \cdot \frac{vP}{\Delta t} \tag{8}$$

where v is in km/s and P and Δt are in seconds. Meanwhile, using the propagation of error formula and defining $C \equiv 4604.66$,

$$\begin{aligned} \sigma_{\text{AU}} &= \sqrt{\left(\frac{d(\text{AU})}{dP}\right)^2 \sigma_P^2 + \left(\frac{d(\text{AU})}{dv}\right)^2 \sigma_v^2 + \left(\frac{d(\text{AU})}{d\Delta t}\right)^2 \sigma_{\Delta t}^2} \\ &= \sqrt{\left(\frac{Cv}{\Delta t}\right)^2 \sigma_P^2 + \left(\frac{CP}{\Delta t}\right)^2 \sigma_v^2 + \left(\frac{-CvP}{(\Delta t)^2}\right)^2 \sigma_{\Delta t}^2} \\ &= \frac{C}{\Delta t}\sqrt{v^2\sigma_P^2 + P^2\sigma_v^2 + \left(\frac{vP}{\Delta t}\right)^2 \sigma_{\Delta t}^2} \end{aligned} \tag{9}$$

Evaluating equations (8) and (9) yields $1 \text{ AU} = 1.69 \pm 0.03 \times 10^8$ km.

VI. CONCLUSION

We successfully estimated the sun's rotation period, rotation speed, and angular size and arrived at a final value for the AU within 15% of the actual value of 1.5×10^8 km.

However, there are ways our methods could be improved. In particular, there are many ways our Doppler shift measurements could be improved. The most obvious drawback is that we did not manage to obtain wavelength solutions for more than one order of the spectrograph, and thus our cross-correlations were limited to a small fraction of the total data.

Additionally, ideally we would perform the Doppler spectroscopy by accounting for the fact that each spectral feature is shifted by a different amount in wavelength space for a given radial velocity, and thus obtain more accurate radial velocity measurements.

We also neglected to take into account the fact that each exposure has some uncertainty in its associated value of $\sin\phi_{obs}$ in Figure 14 (i.e. its position along the apparent solar equator), which originates from the fact that there is an uncertainty in the start time of the transit from fitting the model in section III. Propagating this uncertainty would provide a more complete picture of the uncertainty in fitting our radial velocity model.

Appendix A: Radial Velocity Model

In this section, we describe our method for modeling the observed radial velocity curve for a set of observations transiting the sun's apparent diameter.

To begin, define a coordinate system as shown in Figure 15; the dashed line denotes the path that is traced across the solar disk. The origin is located at the center of the sun (i.e. "inside" the page at a depth of $R_\odot$). The y_{obs} axis lies parallel to the "apparent" equator, i.e. the transit path, and the $\hat{x}_{obs}$ direction points out of the page, toward the observer.

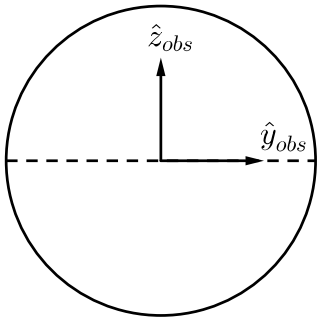

FIG. 15. An observer's coordinate system defined with respect to the image of the solar disk on the sky. The dashed line represents not the true equator of the sun, but the apparent equator, i.e. the path traced by the line of sight as the sun progresses in right-ascension. An x_{obs} axis points out of the page.

We can also define azimuthal and zenith angles in this frame: for any point on the surface of the sun in this frame, ϕ_{obs} is the angle between its x_{obs} and y_{obs} components, and θ_{obs} is the angle between the point's position vector and the z_{obs} axis.

Since each observation is assumed to lie along the apparent equator in this frame, each of the observed points will have $z_{obs} = 0$ and hence $\theta_{obs} = \pi/2$. Thus, a given point's position vector $\vec{p}_{obs}$ will be

$$\vec{p}_{obs} = R_\odot \begin{pmatrix} \cos\phi_{obs} \\ \sin\phi_{obs} \\ 0 \end{pmatrix}$$

where ϕ_{obs} is determined directly from the point's position on the y_{obs} axis and the fact that it must have a component out of the page (i.e along x_{obs}) such that it lies on the surface of the sphere.

Since the sun is tilted with respect to Earth, each point's position vector $(x_{obs}, y_{obs}, z_{obs})$ in the observed frame is actually a transformed version of the point's true position vector (x, y, z)—i.e. its position with respect to the true equator and rotation axis of the sun.

Given a vector $\vec{p} = (x, y, z)$ to a point on the surface of the sun (where x and y lie in the true equatorial plane and z is parallel to the rotation axis), two rotations are performed to obtain its observed counterpart $\vec{p}_{obs}$. First, it is rotated about the y axis by an angle ξ, and then it is rotated about the x axis by an angle η. This is shown in figure 16.

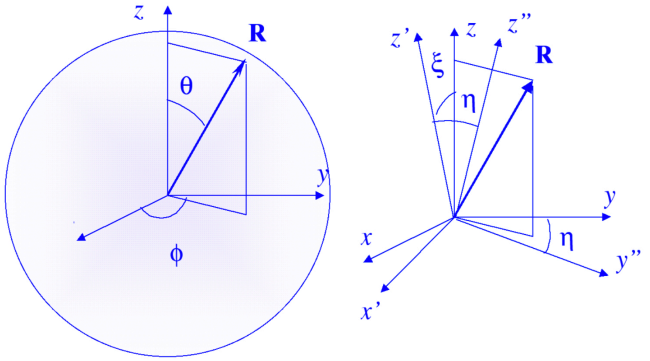

FIG. 16. The true solar equator is not aligned with the "apparent" equator traced out by the line of sight in Figure 15. The true equatorial plane is the x-y plane, and the z axis is the true rotation axis. Any vector defined in the true frame must be rotated first about the y axis and then about the x axis to obtain its observed counterpart. The x', y'', and z'' axes correspond with the x_{obs}, y_{obs}, and z_{obs} axes discussed earlier. Figure from [2].

We can thus define a transformation $\mathbf{M}$ that rotates a velocity or position vector into its observed counterpart:

$$\mathbf{M} \equiv \begin{pmatrix} 1 & 0 & 0 \\ 0 & \cos\eta & \sin\eta \\ 0 & -\sin\eta & \cos\eta \end{pmatrix} \begin{pmatrix} \cos\xi & 0 & \sin\xi \\ 0 & 1 & 0 \\ -\sin\xi & 0 & \cos\xi \end{pmatrix}$$

Therefore, given a vector $\vec{p}_{obs}$, we obtain $\vec{p}$ by $\vec{p} = \mathbf{M}^{-1}\vec{p}_{obs}$. After the transformation is performed, the components of $\vec{p}$ are the x, y, and z values in the "original", i.e. "un-tilted" frame of the sun, shown in the left side of Figure 16. Thus, we can determine the values of θ and ϕ associated with $\vec{p}$, where θ is the angle made with the sun's rotation axis and ϕ is the azimuthal angle in the plane of the sun's equator.

Once θ and ϕ are determined, we find the velocity vector of the point in the same un-tilted frame by

$$\begin{aligned} \vec{v} \equiv \frac{d\vec{p}}{dt} &= R_\odot \frac{d\phi}{dt} \begin{pmatrix} -\sin\theta\sin\phi \\ \sin\theta\cos\phi \\ 0 \end{pmatrix} \\ &= \frac{2\pi R_\odot}{P} \begin{pmatrix} -\sin\theta\sin\phi \\ \sin\theta\cos\phi \\ 0 \end{pmatrix} \end{aligned} \tag{A1}$$

where P is the rotation period, which we have assumed is independent of latitude.

The penultimate step is to transform $\vec{v}$ back to the tilted frame to obtain the observed velocity vector $\vec{v}_{obs} = \mathbf{M}\vec{v}$. Finally, the actual measured radial velocity will be $\vec{v}_{obs} \cdot \hat{x}$, the component of the "tilted" velocity vector along the line of sight. Since $\vec{v}_{obs} \cdot \hat{x}$ is measured, and $\vec{v}_{obs}$ is known up to a constant ($R_\odot$ is unknown), we are thus able to estimate the quantity $2\pi R_\odot/P$, the magnitude of the rotational velocity.

[1] Strong Lines of Neon (Ne). National Institute of Standards and Technology, Physical Measurement Laboratory. https://physics.nist.gov/PhysRefData/Handbook/Tables/neontable2.htm
[2] Graham, James R. Solar Observing. 8 November 2015.